

Phase diagram of the one-dimensional Hubbard model with next-nearest-neighbor hopping

S. Nishimoto,¹ K. Sano,² and Y. Ohta³

¹*Max-Planck-Institut für Physik komplexer Systeme, D-01187 Dresden, Germany*

²*Department of Physics Engineering, Mie University, Tsu 514-8507, Japan*

³*Department of Physics, Chiba University, Chiba 263-8522, Japan*

(Dated: February 2, 2008)

We study the one-dimensional Hubbard model with nearest-neighbor and next-nearest-neighbor hopping integrals by using the density-matrix renormalization group (DMRG) method and Hartree-Fock approximation. Based on the calculated results for the spin gap, total-spin quantum number, and Tomonaga-Luttinger-liquid parameter, we determine the ground-state phase diagram of the model in the entire filling and wide parameter region. We show that, in contrast to the weak-coupling regime where a spin-gapped liquid phase is predicted in the region with four Fermi points, the spin gap vanishes in a substantial region in the strong-coupling regime. It is remarkable that a large variety of phases, such as the paramagnetic metallic phase, spin-gapped liquid phase, singlet and triplet superconducting phases, and fully polarized ferromagnetic phase, appear in such a simple model in the strong-coupling regime.

PACS numbers: 71.10.Pm, 71.10.Fd, 78.30.Jw, 72.15.Nj, 71.30.+h, 71.45.Lr

I. INTRODUCTION

For several decades, quasi-one-dimensional (1D) materials have been one of the major subjects of research in the field of condensed matter physics.^{1,2,3} A standard description of such materials is the 1D Hubbard model.^{4,5,6} The simplest case with the cosine dispersion (nearest-neighbor hopping only) was solved exactly by Lieb and Wu via the Bethe ansatz.⁷ The low-lying excitations were also understood well as the Tomonaga-Luttinger liquid (TLL),⁸ where the renormalization group technique and bosonization method have been used.⁴⁵ However, modifications of the 1D Hubbard model are often required for realistic descriptions of the materials. In general, such modifications (even if they are small) make the analyses much more difficult since the correlation effects are strong in low-dimensional systems. Thus, even in the 1D systems, our knowledge is still far from being complete.

One of the typical modifications is to add a next-nearest-neighbor hopping term in the Hamiltonian, which brings a sort of frustration to the spin degrees of freedom of the system as well as some coupling between spin and charge degrees of freedom. In the past, this model has been extensively studied and some distinctive features, which are absent in the simple 1D Hubbard model, have been found. At half filling, the system has three phases: one is a Mott insulating phase with $2k_F$ spin-density-wave (SDW) correlation (which occurs when the spin frustration is small); the others are a spin-gapped insulating phase with incommensurate spiral correlation and a spin-gapped metallic phase for sufficiently large spin frustration.^{9,10,11,12} Away from half filling, the existence of ferromagnetism has been shown analytically in some limiting cases for infinite strength of the coupling,^{34,35,36} which has been confirmed numerically for finite but large enough strength of the coupling.^{13,14,15} Also, it has been pointed out that, although a weak-

coupling analysis leads to only a spin-singlet superconducting phase with finite spin gap,¹⁷ previous density-matrix renormalization group (DMRG) studies suggest that the spin gap vanishes for large enough coupling strengths when the next-nearest-neighbor hopping is positive and large.^{10,18} Moreover, a spin-triplet superconducting phase has been shown to exist at quarter filling.¹⁹ As just described, the present system has many phases unparalleled in other 1D strongly-correlated electron systems; i.e., our modified 1D model can involve a variety of physical phenomena. In particular, to detect their phases is of particular interest in the light of recent proposals to realize a Hubbard model of fermions on an optical lattice.²⁰

There are some relevant materials to the 1D Hubbard model with next-nearest-neighbor hopping. One is the quasi-1D organic conductor (TMTSF)₂X [X=PF₆, ClO₄], the so-called Bechgaard salt.^{21,22} This material exhibits a rich phase diagram upon variation of the pressure and temperature. At low temperatures, the phase changes in the order as the spin-Peierls insulator, antiferromagnetic insulator, spin-density-wave (SDW) insulator, superconductor, and paramagnetic metal, with increasing pressure. So far, experimental evidence that the superconducting state is in the spin-triplet channel has been piled up.^{23,24} Theoretically, it has been proposed that a triangular lattice formed by the hopping integrals makes the ferromagnetic ring-exchange mechanism relevant, which in turn leads to the spin-triplet superconductivity.²⁵

Another relating system is a newly synthesized copper-oxide compound Pr₂Ba₄Cu₇O_{15- δ} .²⁶ This material consists of both the single CuO chains (as in PrBa₂Cu₃O₇) and double CuO chains (as in PrBa₂Cu₄O₈), and those chains are separated by insulating CuO₂ plains. It has been reported that the double chains turn into a superconducting state below $T_c \sim 10$ K.²⁷ So far, some nu-

merical studies have been carried out; on the basis of the TLL theory, a weak-coupling phase diagram has been obtained in the d - p double chain model.^{28,29} Also, in a reduced single-band double chain model, it has been suggested that the superconducting gap has an extended s -wave-like form, which does not contradict with the experimental results.³⁰ Relevance of charge fluctuations has also been discussed.^{31,32}

In this paper, we study the 1D Hubbard model with the next-nearest-neighbor hopping. We calculate the TLL parameters, spin gap, and total-spin quantum number by using the DMRG method and Hartree-Fock (HF) approximation. Based on the results, a detailed phase diagram as a function of band filling and hopping integrals is determined in both weak-coupling and strong-coupling regimes. Surprisingly, the phase diagram of the model contains a large number of distinct phases in the strong-coupling regime although the model is quite simple. We hope that the present investigation will contribute to better understanding of the 1D strongly-correlated electron systems.

This paper is organized as follows. In Sec. II, we define the 1D Hubbard model with the next-nearest-neighbor hopping and study the model in the noninteracting case. In Sec. III, we discuss how the Hartree-Fock approximation and DMRG method are used to calculate the TLL parameter. In Sec. IV, we present the calculated results and obtain the phase diagrams of the model based on the numerical results. Section V contains summary and conclusions.

II. MODEL

We consider the 1D Hubbard model with the next-nearest-neighbor hopping, which is defined by the Hamiltonian

$$H = t_1 \sum_{i,\sigma} (c_{i+1\sigma}^\dagger c_{i\sigma} + \text{H.c.}) + t_2 \sum_{i,\sigma} (c_{i+2\sigma}^\dagger c_{i\sigma} + \text{H.c.}) + U \sum_i n_{i\uparrow} n_{i\downarrow}, \quad (1)$$

where $c_{i\sigma}^\dagger$ ($c_{i\sigma}$) is the creation (annihilation) operator of an electron with spin σ at site i , and $n_{i\sigma} = c_{i\sigma}^\dagger c_{i\sigma}$ is the number operator. t_1 (> 0) and t_2 are the nearest-neighbor and next-nearest-neighbor hopping integrals, respectively, and U is the on-site Coulomb interaction [see Fig. 1(a)].

The dispersion relation is given by

$$\varepsilon_k = 2t_1 \cos ka + 2t_2 \cos 2ka, \quad (2)$$

where k is the wave number and a is the lattice constant; we set $a = 1$ hereafter. The bare band width is estimated as $W = 2t_1 + 4|t_2| + \frac{t_1^2}{4|t_2|}$ for $|t_2/t_1| \geq 1/2$ and as $W = 4t_1$ for $|t_2/t_1| < 1/2$. The ground-state phase diagram in the noninteracting case ($U = 0$) is shown in

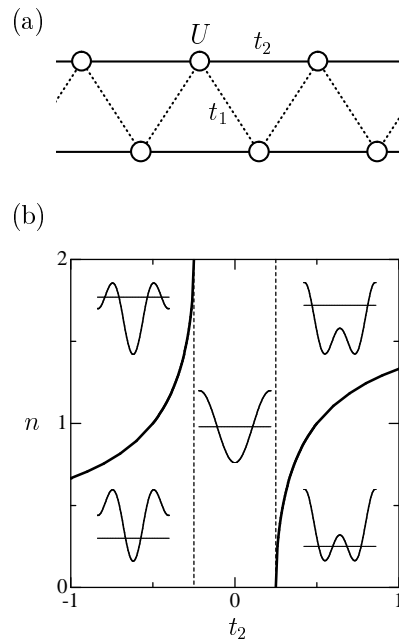


FIG. 1: (a) Schematic representation of the lattice structure of the 1D Hubbard model with the next-nearest-neighbor hopping and (b) its $U = 0$ phase diagram, where the thick solid curves separate the two regimes. The inset shows the qualitative behavior of the band dispersion ε_k , where the Fermi level is indicated by the thin line.

Fig. 1(b). For $|t_2/t_1| < \cos^2[(2-n)\pi/2]/\sin^2[(2-n)\pi]$ (n is the band filling), the system has two Fermi points and the physical properties at low energies are qualitatively the same as a system with $t_2 = 0$. On the other hand, for $|t_2/t_1| > \cos^2[(2-n)\pi/2]/\sin^2[(2-n)\pi]$, there are two branches, namely four Fermi momenta $\pm k_{F1}$ and $\pm k_{F2}$ ($|k_{F2}| > |k_{F1}|$). In this case, as discussed in Sec. IV.A, the Fermi surface can be mapped to that of a two-leg Hubbard ladder model at weak coupling. We designate the critical boundary at which the Fermi surface splits into four points as the Fermi-point (FP) boundary and the FP boundary is characterized by a condition $k_{F1} = 0$ (or $k_{F2} = \pi$). Hence, the model (1) has to be dealt with as a two band system within the TLL theory. Note that the parameter region $n > 1$, $t_2 > 0$ is exactly equivalent to the region $n < 1$, $t_2 < 0$ under the particle-hole transformation. By the same token, the region $n < 1$, $t_2 > 0$ equals to the region $n > 1$, $t_2 < 0$. We therefore consider only the region $0 < n \leq 1$ for both positive and negative values of t_2 .

III. METHOD

The low-energy properties of TLL are characterized by a few quantities; most notably, the TLL parameter K_ρ determines the long-range behavior of various correlation functions in the metallic TLL ground state. It has however been recognized that the numerical calculation of

K_ρ for an arbitrary strength of correlations is very difficult. Recently, one of the authors has succeeded to overcome this difficulty,⁴⁰ where a simple and stable method for calculating K_ρ with the DMRG technique in single-band 1D systems is proposed. In this section, we extend the method to the two-band systems and check the performance of the method by comparing the results with those obtained by the HF approximation which is known to provide a good estimation of K_ρ in the weak-coupling regime.

A. HF approximation

It is known that the small- U perturbative estimation of K_ρ is feasible for $U \lesssim W/2$ in the 1D Hubbard model.³⁷ One of the authors applied this perturbative method to a two-leg Hubbard ladder model with four Fermi points and confirmed that it gives quantitatively reliable results in the weak-coupling regime ($U \lesssim W/4$).³⁸ Since the low-energy physics of the two-leg ladders is equivalent to that of our model defined by Eq. (1),¹⁷ we may naturally expect the perturbative estimation to be applicable to our case.

In the TLL theory, the critical exponent K_ρ is given by

$$K_\rho = \frac{1}{2} \sqrt{\pi \chi D}, \quad (3)$$

where χ is the charge susceptibility defined as

$$\chi^{-1} = \frac{1}{L} \frac{\partial^2 E_{\text{gs}}(n)}{\partial n^2}, \quad (4)$$

and D is the Drude weight defined as

$$D = \frac{\pi}{L} \frac{\partial^2 E_{\text{gs}}(\phi)}{\partial \phi^2}. \quad (5)$$

Here, L is the number of lattice site, n is the band filling, E_{gs} is the ground-state energy, and ϕ is the magnetic flux.³⁹ Within the first-order perturbation expansion, E_{gs} can be determined as

$$E_{\text{gs}} = E_0 + \frac{UL}{4} n^2 \quad (6)$$

where E_0 is the ground-state energy of the corresponding noninteracting system. We then obtain

$$\chi^{-1} = \chi_0^{-1} + \frac{U}{2}, \quad D = D_0 = \frac{4\chi_0^{-1}}{\pi} \quad (7)$$

where χ_0 and D_0 are the charge susceptibility and Drude weight of the noninteracting system, respectively. A simple expression for K_ρ is therefore obtained as

$$K_\rho \simeq \sqrt{\frac{2}{2 + U\chi_0}}. \quad (8)$$

Note that this scheme is equivalent to the HF approximation.³⁸

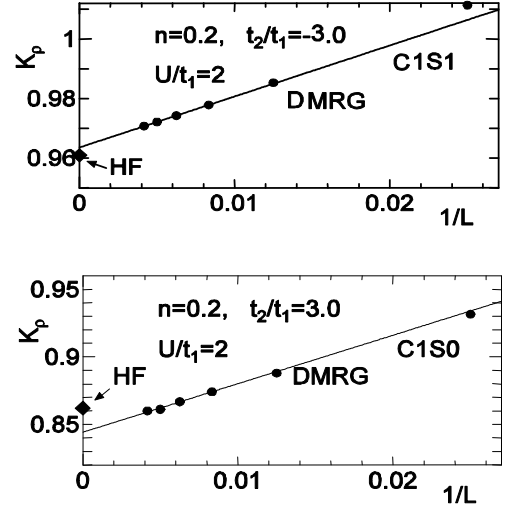


FIG. 2: Values of $K_\rho(L)$ calculated by the DMRG method and plotted as a function of the inverse system size $1/L$. Solid lines are the polynomial fits to the data for finite-size scaling analysis. Diamonds indicate the results calculated from the Hartree-Fock approximation. The upper and lower panels show the result at $t_2/t_1 = -3$ and $t_2/t_1 = 3$, respectively. $U/t_1 = 2$ and $n = 0.2$ are assumed in both panels.

B. DMRG

With the DMRG method, the TLL parameter K_ρ is most generally obtained from the long-range decay of the density-density correlation. The density-density correlation function is defined by the ground-state expectation value

$$C^{\text{NN}}(r) = \frac{1}{L} \sum_{l=1}^L (\langle n_{l+r} n_l \rangle - \langle n_{l+r} \rangle \langle n_l \rangle). \quad (9)$$

When the system has two Fermi points, it is known that the asymptotic behavior is given by

$$C^{\text{NN}}(r) \sim -\frac{K_\rho}{(\pi r)^2} + \frac{A \cos(2k_F r)}{r^{1+K_\rho}} \ln^{-3/2}(r) + \dots, \quad (10)$$

where A is a constant.^{37,41} We can extract K_ρ via the Fourier transformation of Eq. (9),

$$C^{\text{NN}}(q) = \frac{1}{L} \sum_{l=1}^L e^{-iqr} C^{\text{NN}}(r), \quad (11)$$

where $0 \leq q < 2\pi$. From the derivative at $q = 0$, one finds the expression

$$K_\rho(L) = \frac{L}{2} C^{\text{NN}} \left(\frac{2\pi}{L} \right), \quad K_\rho = \lim_{L \rightarrow \infty} K_\rho(L). \quad (12)$$

for the thermodynamic limit. It has been demonstrated that the value of K_ρ can be determined quite accurately by using Eq. (12) with the DMRG method for the single-band Hubbard model. Thus, for the precise estimation,

we need to calculate the density-density correlation function directly in the Fourier space; see Ref. 40 for further details.

Let us now apply this scheme of estimating K_ρ to a system with four Fermi points. We then have to assume the asymptotic behavior of the density-density correlation function. Here we assume the behavior

$$C^{\text{NN}}(r) \sim -\frac{2K_\rho}{(\pi r)^2} + \frac{B \cos[2(k_{\text{F}1} - k_{\text{F}2})r]}{r^{2k_\rho}} + \dots, \quad (13)$$

in analogy with the case of two coupled chains,⁴² because the calculated low-energy excitation spectra of our model are similar to those of the two coupled chains.⁴³ We thus obtain

$$K_\rho(L) = \frac{L}{4} C^{\text{NN}}\left(\frac{2\pi}{L}\right), \quad K_\rho = \lim_{L \rightarrow \infty} K_\rho(L), \quad (14)$$

as a substitute for Eq. (12). In principle, one may calculate Eq. (14) in the same way as Eq. (12). However, the discarded weight in the DMRG calculation increases rapidly with increasing $|t_2/t_1|$, so that the calculation must be carried out more carefully.

In this paper, we apply the open-end boundary conditions for precise DMRG calculations.⁴⁴ We keep up to $m \simeq 4500$ density-matrix eigenstates in the DMRG procedure and extrapolate the calculated quantities to the limit $m \rightarrow \infty$. We also use several chains with lengths $L = 40$ to 240 and then perform the finite-size scaling analysis based on the size-dependence of the quantities. In this way, we can obtain the quite accurate ground state with an accuracy of $\Delta E_{\text{gs}}/L \sim 10^{-6} - 10^{-5} t_1$. In Fig. 2, we demonstrate the finite-size scaling analysis for (a) the two- and (b) four-Fermi point cases. For both cases, one can see the systematic extrapolation of K_ρ to the thermodynamic limit $L \rightarrow \infty$. We also find that, at least in this coupling strength $U/t_1 = 2$, a good agreement is obtained between the extrapolated values of K_ρ obtained from the DMRG data and the corresponding values of K_ρ obtained from the HF approximation.

IV. RESULTS

A. Weak-coupling limit

Let us first consider the phase diagram within a weak-coupling analysis. Balents and Fisher have obtained the weak-coupling phase diagram of the two-leg Hubbard ladder model using the renormalization group technique and bosonization method.⁴⁵ Their analysis can be universally applied to a system with four Fermi points. In addition, Fabrizio pointed out¹⁷ that the low-energy physics of the two-leg Hubbard ladder model is exactly the same as that of our model (1) via a simple mapping of the Fermi points, i.e., $\pm k_{\text{F}1} \rightarrow \mp k_{\text{F}}^a$ and $\pm k_{\text{F}2} \rightarrow \mp k_{\text{F}}^b$ where $\pm k_{\text{F}}^a$ ($\pm k_{\text{F}}^b$) are the Fermi points for the antibonding (bonding) band of the two-leg Hubbard ladder model. Then,

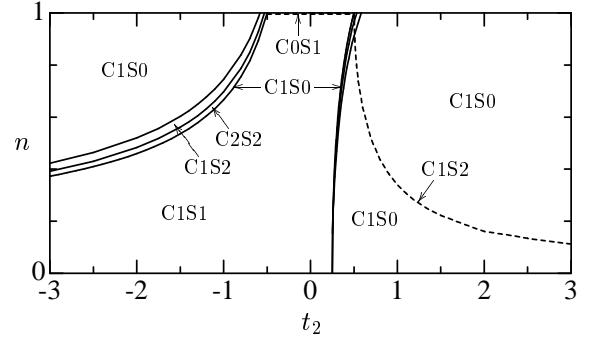


FIG. 3: Phase diagram of our model in the weak-coupling limit $U = 0^+$. We follow the notation of the symbol $\text{C}\alpha\text{S}\beta$ of Ref.⁴⁵.

Daul and Noack adapted the weak-coupling analysis of Ref. 45 for the analysis of the Hamiltonian (1).¹⁶

In Fig. 3, we show the phase diagram for $|t_2/t_1| < 3$ and $n < 1$ in the weak-coupling limit $U = 0^+$. A notation $\text{C}\alpha\text{S}\beta$ denotes a phase with α gapless charge modes and β gapless spin modes, where α and β are integer values from 0 to 2. Generally speaking, a metallic phase with four (two) Fermi points is characterized by C1S0 (C1S1). Also, a spin-gapped liquid phase C1S0 appears around the FP critical boundary due to the van Hove singularity of the model. Note that the TLL parameter has the value $K_\rho = 1$ in nearly all the metallic regimes, except at the FP critical boundary and on the C0S1 line, where we have $K_\rho = 1/2$.

B. Small U

Let us turn to the small- U perturbative regime where we choose the coupling strength $U = 2t_1$. In this regime, the HF estimation of K_ρ [Eq.(8)] is expected to give a good approximation. When the system has two Fermi points, we can simply obtain

$$\chi_0^{-1} = \frac{\pi}{2} v_{\text{F}}, \quad (15)$$

which leads to

$$K_\rho = \sqrt{\frac{\pi v_{\text{F}}}{\pi v_{\text{F}} + U}} \quad (16)$$

where the Fermi velocity is

$$v_{\text{F}} = 2t_1 \sin(\pi n/2) - 4t_2 \sin(\pi n). \quad (17)$$

This expression (16) is universal to the TLL with two Fermi points. On the other hand, when the system has four Fermi points, we obtain

$$\chi_0^{-1} = \frac{\pi}{2} \frac{|v_{\text{F}1} v_{\text{F}2}|}{|v_{\text{F}1}| + |v_{\text{F}2}|} \quad (18)$$

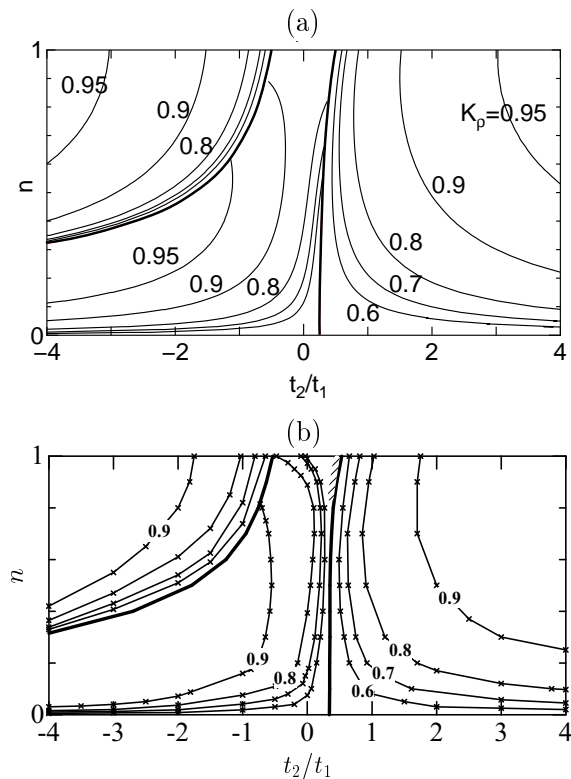


FIG. 4: Contour map of the TLL parameter K_ρ in the $n-t_2/t_1$ plane for the weak-coupling interaction $U = 2t_1$. The results are obtained from (a) the HF and (b) DMRG calculations. The thick line represents the FP critical boundary.

after some calculations, where v_{F1} (v_{F2}) is the Fermi velocity at the momentum k_{F1} (k_{F2}) given as

$$v_{F(1,2)} = 2t_1 \sin(k_{F(1,2)}a) - 4t_2 \sin(2k_{F(1,2)}a). \quad (19)$$

Substituting Eq. (18) for Eq. (8), we obtain

$$K_\rho = \sqrt{\frac{\pi v_F^*}{\pi v_F^* + U}} \quad (20)$$

with using an effective Fermi velocity

$$v_F^* \equiv \frac{|v_{F1}v_{F2}|}{|v_{F1}| + |v_{F2}|}. \quad (21)$$

In Fig. 4, we show the contour maps of K_ρ at $U = 2t_1$ in the parameter space of t_2/t_1 and n , which are calculated with (a) the HF approximation and (b) the DMRG method. The thick line represents the FP critical boundary and the thin lines form the contour map of K_ρ . We find that the quantitative agreement between the two phase diagrams is pretty good, which means that the HF scheme is still valid for this interaction strength $U/t_1 = 2$. In the entire region of the phase diagram, we find $K_\rho > 1/2$ and thus the ground state may be described as the TLL. However, the deviation of the HF data from the DMRG data is relatively large around $t_2 \approx 0$ and $n \approx 1$, where the umklapp scattering becomes dominant.

When the system has two Fermi points, the ground state can basically be presumed to be a standard 1D TLL. In both contour maps, K_ρ becomes larger as t_2 decreases for fixed n . This is because the effective interaction parameter U/v_F is reduced with decreasing t_2 . In particular, K_ρ varies drastically around $t_2 \sim 0$ except when $n \lesssim 0.1$ and $n \gtrsim 0.9$, which is due to the rapid change of the inverse Fermi velocity v_F^{-1} ; for example, the Fermi velocity is estimated as $v_F = \sqrt{2}t_1 - 4t_2$ at quarter filling ($n = 1/2$). Note that $K_\rho = 1/2$ is reached in the limits $n \rightarrow 0$ and 1 and that $K_\rho > 1/2$ everywhere else.

As soon as the Fermi surface splits from two into four points, K_ρ drops (almost) discontinuously to $1/2$. When the system has four Fermi points, v_F^* goes to zero in the limits $v_{F1} \rightarrow 0$ ($k_{F1} \rightarrow 0$) or $v_{F2} \rightarrow 0$ ($k_{F2} \rightarrow \pi$) [corresponding to the diverging density of states]. Consequently, the effective interaction parameter diverges, $U/v_F^* \rightarrow \infty$, and the strong-coupling value $K_\rho = 1/2$ is produced. This behavior is similar to that of the 1D single-band Hubbard model in the limit of $n \rightarrow 0$. Then, K_ρ increases rapidly as the parameters are away from the FP boundary line and gets closer to 1 in the limit of $|t_2| \rightarrow \infty$. In the two-band model, the criterion for the dominant superconducting correlation is $K_\rho > 1/2$. We thus find that the superconducting correlation is the most dominant in the entire region with four Fermi points.

C. Large U

Let us now consider how the small- U contour map is affected by increasing the strength of the on-site Coulomb interaction. For large enough coupling U , it has been found that there is an extensive ferromagnetic phase^{13,14,15} and that the spin-triplet superconducting state is stabilized at the intermediate filling $n \sim 0.5$ when the next-nearest-neighbor hopping is large enough, $t_2/t_1 \gtrsim 2$.¹⁹ A breakdown of the TLL state was also reported for the 1D Hubbard and $t-J$ models with the next-nearest-neighbor hopping integrals,^{46,47} where the latter model is essentially the same as our model (1) in the strong-coupling regime.

We here study the case of $U = 10t_1$ as a typical interaction strength for realistic strongly-correlated electron systems. In Fig. 5, we show the contour map of K_ρ obtained by (a) the HF approximation and (b) DMRG method. We find that, at low densities ($n \lesssim 0.4$), the agreement between the two contour maps is qualitatively good, while at intermediate to high densities ($n \gtrsim 0.4$), the situation seems to be totally different. In fact, the HF scheme is no longer appropriate and therefore the spin and charge fluctuations have to be taken seriously into account beyond the usual weak-coupling picture. We will thus proceed to a discussion based on the DMRG contour map in the following.

We first note that, as far as the system has two Fermi points, the basic properties are qualitatively the same as

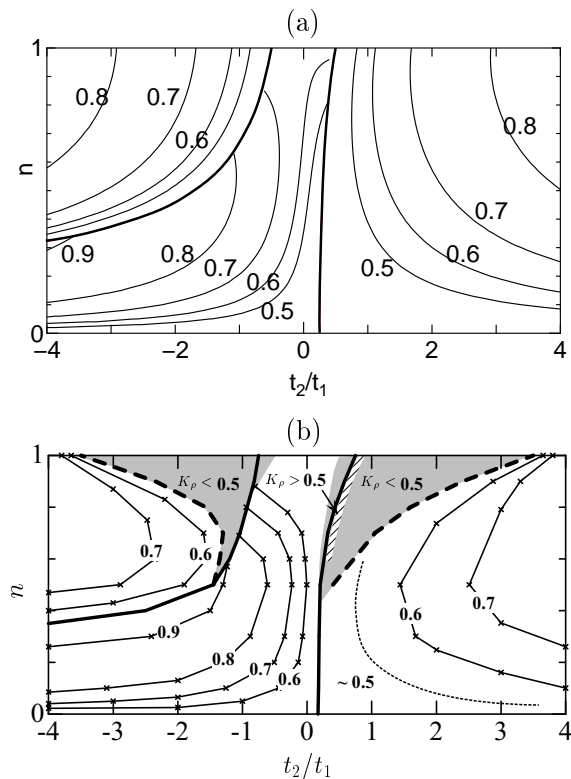


FIG. 5: Contour map of the TLL parameter K_ρ in the n - t_2/t_1 plane for the strong-coupling interaction $U = 10t_1$. The results are obtained from (a) the HF and (b) DMRG calculations. The thick line represents the FP critical boundary.

those of the weak-coupling regime. Thus, the behavior of K_ρ at $U = 10t_1$ is still similar to that at $U = 2t_1$ although the value of K_ρ becomes relatively small. We also note that the FP boundary is (slightly) shifted toward the smaller $|t_2|$ direction due to renormalization of the band structure at $U > 0$, as was pointed out in Ref. 16. At the same time, the FP boundary line is somewhat blurred because of some strong quantum effects; the change in K_ρ at the FP boundary is still sharp but no longer discontinuous as in the weak-coupling limit.

Let us turn to the case with four Fermi points. The ground state is affected drastically by the (strong) interaction strength. Unlike in the small- U contour map, we find that there is a substantial region with $K_\rho < 0.5$ around half filling [denoted by the shadowed area in Fig. 5(b)]. According to the TLL theory, this value of K_ρ is possible only when long-range repulsive interactions are included in the model. Therefore, the ground state in the shadowed regime would no longer belong to the general class of the TLLs. This is consistent with the previous DMRG results.^{16,47} As discussed in the next subsection, this non-TLL-like regime consists of a spin-gapped phase and a paramagnetic phase with strong ferromagnetic fluctuations. Also, it is interesting to note that the TLL parameter remains constant $K_\rho \sim 0.5$ in a wide region of the phase diagram near the FP boundary

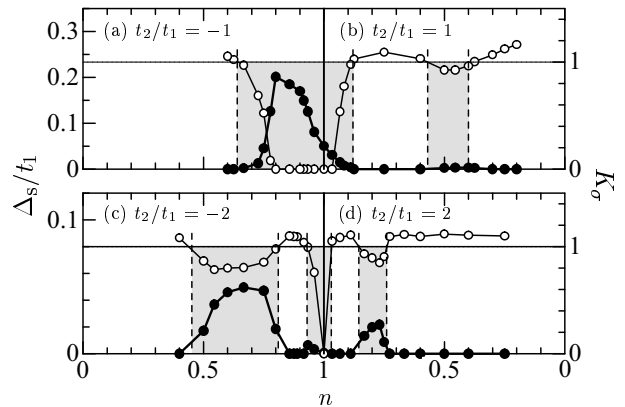


FIG. 6: Calculated values of the spin gap (solid symbols, left axis) and TLL spin exponent (open symbols, right axis) at (a) $t_2/t_1 = -1$, (b) 1, (c) -2, and (d) 2. $U/t_1 = 10$ is assumed. The solid line denotes $K_\sigma = 1$ and the vertical dotted lines indicate the critical boundaries between the presence and absence of the spin gap.

at low densities.

Furthermore, it is particularly worth noting that K_ρ seems to be enhanced significantly at the FP boundary near half filling. [In this area, precise evaluation of K_ρ in the thermodynamic limit $1/L \rightarrow 0$ is rather hard because $|\partial K_\rho(L)/\partial(1/L)|$ increases with decreasing the inverse system size $1/L$.] If the definition (3) could be still valid in this region, K_ρ become quite large > 1 : for the van Hove singularity, the charge susceptibility χ in Eq. (4) can diverge and the Drude weight D in Eq. (5) must remain finite. This may be associated with the C1S0 phase attributed to the van Hove singularity at $k_{F1} = 0$ (or $k_{F2} = \pi$) in the weak-coupling phase diagram. This is consistent with a prediction that the superconducting fluctuations increase with increasing the difference between $|v_{F1}|$ and $|v_{F2}|$, as was suggested in Ref. 45.

D. Spin gap

For more elaborate studies of the region with four Fermi points, we consider the spin degrees of freedom in the strong-coupling regime $U = 10t_1$. Of particular interest here is the presence or absence of a finite energy gap in the spin excitation spectrum. We thus evaluate the spin gap defined by an energy difference between the first spin-triplet excited state and the singlet ground state: i.e.,

$$\Delta_s = \lim_{L \rightarrow \infty} [E_{\text{gs}}(N, 1) - E_{\text{gs}}(N, 0)], \quad (22)$$

where $E_{\text{gs}}(N, S_z)$ is the ground-state energy for a given number of electrons N and z-component of the total spin S_z . It is however known that, for some parameter values, the spin gap becomes too small to figure out if it remains finite, e.g., $\Delta_s \lesssim 10^{-3}t_1$. For verifying the presence or

absence of the spin gap, we then calculate the TLL spin exponents, which is given by

$$K_\sigma = \lim_{L \rightarrow \infty} \frac{L}{2} \sum_{kl} e^{i \frac{2\pi}{L}(k-l)} \langle S_k^z S_l^z \rangle \quad (23)$$

where $S_i^z = n_{i\uparrow} - n_{i\downarrow}$. We should find that the spin exponent takes the value $K_\sigma = 0$ in the spin-gapped phase and $K_\sigma = 1$ everywhere else in the thermodynamic limit.⁵³ However, for finite-size systems, the situation is not so simple. In practice, in the spin-gapless phase, one cannot expect to find the value $K_\sigma \rightarrow 1$ due to the logarithmic corrections. It is known that the logarithmic corrections vanish at which the spin gap opens, in analogy with the dimerization transition in the J_1 - J_2 model [see Eq. (24) below].⁵¹ Also, in the spin-gapped phase, if the spin gap is very small, the convergence of K_σ to 0 will obviously occur only for very large systems. Therefore, we here determine the critical point at which the spin gap opens by adopting the condition that the value of K_ρ crosses 1. This method was first proven to be useful in Ref.⁴⁸ In Fig. 6(a)-(d), the spin gap and TLL spin exponent calculated by the DMRG method are plotted as a function of the band filling n for various t_2/t_1 values.

For $U \gg t_1, t_2$, our model (1) at half filling can be mapped onto a Heisenberg model

$$H = J_1 \sum_i \vec{S}_i \cdot \vec{S}_{i+1} + J_2 \sum_i \vec{S}_i \cdot \vec{S}_{i+2} \quad (24)$$

with $J_1 = 4t_1^2/U$ and $J_2 = 4t_2^2/U$. This model has been extensively studied both analytically^{49,50,51,52} and numerically.^{10,18} It has been found that the spin gap opens when $J_2/J_1 \geq 0.241$; the ground state is of a dimerized zigzag-bond state for $0.241 \leq J_2/J_1 \lesssim 0.5$ and of the Majumdar-Ghosh state with incommensurate spiral correlations for $J_2/J_1 \gtrsim 0.5$. For example, the spin gap was estimated to be $\Delta_s \simeq 0.25J_1$ at $J_2/J_1 \sim (t_2/t_1)^2 = 1$ in the previous DMRG study.⁵² This value is comparable to our estimation $\Delta_s/t_1 \simeq 0.05$ for $t_2/t_1 = 1$ and $U = 10t_1$. Also, the spin gap is of an exponential dependence on J_2/J_1 as $\Delta_s \propto \exp(-\text{const.} \times J_2/J_1)$ for large J_2/J_1 values, which is consistent with a very small spin gap $\Delta_s/t_1 \sim 0.0005$ for $t_2/t_1 = 2$ and $U = 10t_1$ obtained in our calculations.

Let us turn to the evolution of the spin gap upon doping. In the weak-coupling phase diagram, a metallic phase with four (two) Fermi points is simply characterized as the spin-gapped (gapless) TLL. However, for large U values, it is difficult to speculate the n -dependence of the spin gap because of the competition between the anti-ferromagnetic exchange interaction and two kinds of the ferromagnetic interactions; One is induced by the Nagaoka mechanism, which leads to long-range ferromagnetic fluctuations for slightly-doped systems,^{33,34} where the mechanism is known to work even for finite doping levels.^{36,55} The other is the three-site ring-exchange mechanism, which yields ferromagnetic spin correlations for the intermediate filling.¹⁹ This mechanism works only

when the product of three hopping integrals along the triangles forming the triangular lattice is positive, i.e., $t_1^2 t_2 > 0$ in our system [see, Fig. 1(a)]. Away from half filling, the spin gap has so far been calculated with the DMRG methods for some parameters,^{16,19,54} and we now study the spin gap in a wider range of the n - t_2/t_1 plane. The results are the following:

(i) For $t_2/t_1 = -1$, $n < 1$ [Fig. 6(a)], the spin gap is considerably enhanced with decreasing n near half filling. Since the geometrical spin frustration is reduced by doping, the spin-singlet bound state is in a better position to be formed. The value of Δ_s increases rapidly as n decreases, reaches the maximum value $\Delta_s/t_1 \sim 0.2$ around $n \sim 0.8$, and goes down to zero at the FP boundary $n \sim 0.64$. The spin gap is always zero when the system has two Fermi points, which is in agreement with the weak-coupling phase diagram. We should note that no singularity in the spin gap is found at half filling.

(ii) For $t_2/t_1 = -2$, $n < 1$ [Fig. 6(c)], the spin gap is enhanced by doping in the vicinity of half filling as in the case of (i). However, unlike in the case (i), the spin gap vanishes around $n \sim 0.93$ even though the system has still four Fermi points. This may be related to the ferromagnetic spin fluctuations induced by the Nagaoka mechanism. Thus, the region for $0.81 \lesssim n \lesssim 0.93$ is spin gapless. Further away from half filling, the Nagaoka mechanism can no longer work well and the ferromagnetic fluctuations weaken. Consequently, the spin gap opens again in the filling from $n \sim 0.81$ to the FP critical boundary $n \sim 0.45$. It is also interesting to note that the critical filling $n \sim 0.81$ agrees with the TLL critical boundary; i.e., the spin gap starts to open at the point of $K_\rho = 0.5$.

(iii) For $t_2/t_1 = 1$, $n < 1$ [Fig. 6(b)], the spin gap is always finite for small U values [see Ref.16]. For large U values, however, the spin gap behaves intricately as a function of doping due to the existence of two types of the ferromagnetic fluctuations. Near half filling, Δ_s decreases with decreasing n and disappears around $n \sim 0.88$. We can see that no spin gap exists in a region $0.57 \lesssim n \lesssim 0.88$. This is consistent with the fact that the critical interaction strength U_c at the ferromagnetic transition is relatively small for this region,¹⁶ which would indicate the strong ferromagnetic fluctuations there. And then, with decreasing n , the spin gap opens again around $n \sim 0.57$, where the Nagaoka mechanism no longer works well. Like in the case (ii), the point where the spin gap opens is on the TLL critical boundary. By further doping, the spin gap closes around $n \sim 0.4$. For $n \lesssim 0.4$, the spin gap is zero due to the ferromagnetic fluctuations induced by the three-site ring-exchange interaction. Note that there is no spin gapless region derived by the three-site ring-exchange interaction in the case of (ii) where $t_1^2 t_2 < 0$.

(iv) For $t_2/t_1 = 2$, $n < 1$ [Fig. 6(d)], the properties are qualitatively the same as in the case of (iii). The spin gap remains finite only for a tiny region in the vicinity of half filling ($n \gtrsim 0.97$) and for a small region adjacent to the TLL critical boundary ($0.74 \lesssim n \lesssim 0.85$). The

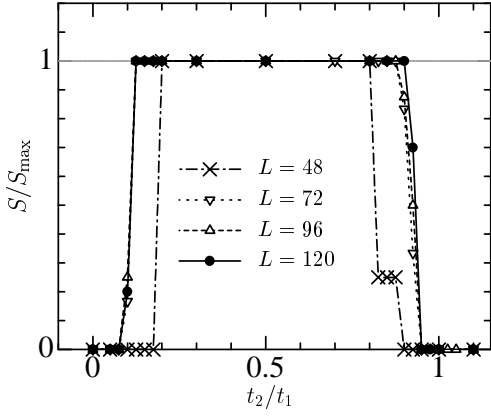


FIG. 7: Calculated values of the total-spin quantum number S as a function of t_2/t_1 for various system sizes L . $U/t_1 = 10$ and $n = 1/6$ are assumed.

three-site ring-exchange interaction is more robust than in the case of (iii),¹⁹ so that the gapless area becomes wider ($n \lesssim 0.74$).

E. Fully polarized state

Of further interest is the presence of the fully polarized ferromagnetic state, which occurs when t_2 is positive in the strong-coupling regime. Previously, for $U = \infty$, ferromagnetism has been analytically shown to exist in the three limiting cases: $n \rightarrow 1$,³⁴ $t_2 \rightarrow 0$,³⁵ and $n \rightarrow 0$.³⁶ Also, for finite U values, it has been shown numerically that there is an extensive ferromagnetic phase, where the exact diagonalization,¹³ variational,¹⁴ and DMRG¹⁵ methods have been used.

Let us then investigate how the ferromagnetic phase appears in the phase diagram. We can find it by calculating the expectation value of total-spin operator \vec{S} in the ground state, which is defined by

$$\langle \vec{S}^2 \rangle = \sum_{ij} \langle \vec{S}_i \cdot \vec{S}_j \rangle = S(S+1). \quad (25)$$

For a fully-polarized state, one will obtain $S = S_{\max} = N/2$, i.e., $S/S_{\max} = 1$. In Fig. 7, we show the total spin S normalized with respect to S_{\max} as a function of t_2/t_1 at $U = 10$ and $n = 1/6$ for various system sizes. We can see a transition between paramagnetic and ferromagnetic states at $(t_2/t_1)_c \sim 0.1$ and 0.95 . The change in S/S_{\max} at $(t_2/t_1)_c$ becomes sharper with increasing L , suggesting the transition to be (almost) discontinuous for $L > 72$. Therefore, the transition may be of the first-order in the thermodynamic limit. Thus, the critical transition point can be determined in the parameter space, which will be given in the next subsection.

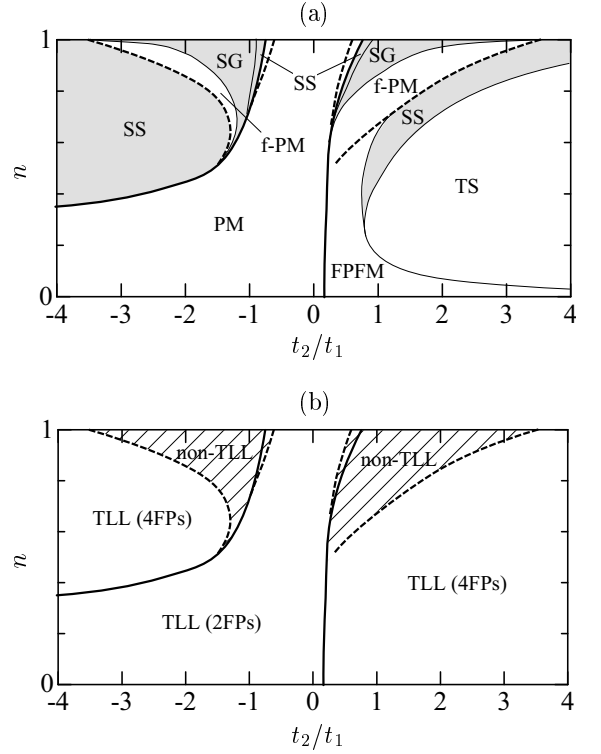


FIG. 8: (a) Ground-state phase diagram of the 1D Hubbard model with the next-nearest-neighbor hopping, calculated by the DMRG method. $U/t_1 = 10$ is assumed. The bold (dotted) line indicates the FP (TLL) critical boundary and the shaded area represents a spin-gapped phase. We use the following abbreviations; PM: paramagnetic metal, SG: spin-gapped liquid with incommensurate spiral correlations, f-PM: paramagnetic metal with strong ferromagnetic fluctuations, FPFM: fully polarized ferromagnetic metal, and SS (TS): spin-singlet (triplet) superconductivity. (b) Boundary lines between the TLL and non-TLL-like regions.

F. Phase diagram

Based on the calculated results of the TLL parameters $K_{\rho,\sigma}$, spin gap Δ_s , and total-spin quantum number S , we draw a $U = 10$ phase diagram of the 1D Hubbard model with the next-nearest-neighbor hopping. The result is shown in Fig. 8(a). We find that our system Eq. (1) exhibits a variety of phases in the parameter space of t_2/t_1 and n ; it includes a paramagnetic metal (PM), a spin-gapped liquid with incommensurate spiral correlations (SG), a paramagnetic metal with strong ferromagnetic fluctuations (f-PM), a fully-polarized ferromagnetic metal (FPFM), a spin-singlet superconductivity (SS), and a spin-triplet superconductivity (TS). The bold and dotted lines in Fig. 8(a) indicate the FP and TLL critical boundary, respectively, and the shaded area represents a spin-gapped phase.

When the system has two Fermi points, the ground-state properties are essentially the same as those of the standard 1D Hubbard model with $t_2 = 0$. The system

is thus a paramagnetic metal with $0.5 < K_\rho < 1$, where the $2k_F$ -SDW correlation is most dominant. The introduction of t_2 brings a sort of frustration to the $2k_F$ -SDW oscillation, but the oscillation is never broken down as long as the system has two Fermi points.

We now turn to the region with four Fermi points. As shown in Sec. IV. D, this region consists of the TLL ($K_\rho \geq 1/2$) and non-TLL-like ($K_\rho < 1/2$) phases [see Fig. 8(b)]. Looking first at the TLL phase with $K_\rho > 1/2$, the superconducting correlation is most dominant according to the TLL theory. The superconducting phase for $t_2 > 0$ is further divided into a couple of phases, depending on the presence or absence of the spin gap; the spin-gapless phase extends over a wide range for large t_2 , which is in contrast to the weak-coupling phase diagram. This spin-gapless area seems to be expanded by increasing the on-site interaction U , as compared to the previous DMRG results for $U = 2t_1$.¹⁰ [In Ref.10, this phase is characterized as $2 \times \text{C1S1} = \text{C2S2}$.] The ground state is featured as the spin-triplet superconductivity, as has been confirmed numerically.¹⁹ On the other hand, the spin-gapped phase is characterized by the spin-singlet superconductivity, which is remnant of a wide C1S0 region in the weak-coupling phase diagram. It is particularly worth noting that the TLL phase for $t_2 < 0$ is always spin-gapped and the spin-singlet superconducting correlation is most dominant. This is consistent with the fact that the three-site ring-exchange interaction for spin-triplet coupling does not work if $t_1^2 t_2 < 0$.

The other TLL phase belongs to the fully-polarized ferromagnetic metal near the FP boundary and at low densities. A nearly flat-band system is realized since the two band minima are slightly occupied by electrons at low densities (or the band maximum at $k = 0$ is slightly occupied by holes near the FP boundary). Consequently, the ferromagnetic ground state is stabilized. In the FPFM phase, we estimate the TLL parameter as $K_\rho \sim 0.5$ [see Fig. 5(b)], which is the same as that of a spinless fermion system.

We next consider the non-TLL-like regime, which extends between the TLL region and the half-filling line. The paramagnetic phase with strong ferromagnetic correlation is located in the vicinity of the TLL regime, where the ferromagnetic fluctuations are enhanced due to the Nagaoka mechanism; this phase is denoted as f-PM in Fig. 7. At present value of U , the total spin of the ground state is zero in the entire area of the f-PM phase. As U increases, the f-PM phase is enlarged and the system would be fully polarized at a critical value of U .

Further approaching the vicinity of $n = 1$, the spin-gapped region appears again. Although most of the spin-gapped region is paramagnetic, a narrow spin-singlet superconducting phase with $K_\rho > 0.5$ exists along the FP boundary line. We can interpret this situation by assuming the system to be a slightly doped J_1 - J_2 Heisenberg model (24): for $J_2/J_1 \gtrsim 0.5$, the ground state is of the Majumdar-Ghosh state with incommensurate spiral cor-

relations and the spin-singlet bound state is formed along the t_2 -chains, where the spin-singlet bound state cannot easily move. On the other hand, for $0.241 \leq J_2/J_1 \lesssim 0.5$, the ground state is of a dimerized zigzag-bond state where the spin-singlet bound state is formed between the two t_2 -chains. At finite doping levels of holes, the spin-singlet pairs are mobile in this region, so that in the ground state an additional pair of holes is actually confined to a ‘rung’ because the gain in kinetic energy due to the hole motion is larger than the combined loss in the pairing energy and kinetic energy of the spin dimers in the Majumdar-Ghosh state. Thus, the narrow spin-singlet superconducting state can be regarded as the doped zigzag-bond state.

V. SUMMARY

We have studied the 1D Hubbard model with the nearest-neighbor and next-nearest-neighbor hopping integrals by using the DMRG method and HF approximation. Based on the calculated results of the TLL parameters, spin gap, and total-spin quantum number, we have determined the ground-state phase diagrams in the weak-coupling ($U = 2t_1$) and strong-coupling ($U = 10t_1$) regimes. Surprisingly, the strong-coupling phase diagram contains a large variety of distinct phases, depending on the hopping integrals and band filling.

We have found for $U = 2t_1$ that the HF results agrees well with the DMRG results except for $t_2 \approx 0$ and $n \approx 1$ where the umklapp scattering strength is dominant. The phase diagram is qualitatively the same as that in the weak-coupling limit. When the system has two Fermi points, the $2k_F$ -SDW correlation is most dominant with $1/2 < K_\rho < 1$. As soon as the Fermi surface splits from two into four points, the parameter K_ρ drops (almost) discontinuously to $1/2$. We then have found $K_\rho > 1/2$ in the entire region with four Fermi points and thus the superconducting correlation is most dominant.

We have then found for $U = 10t_1$ that the HF results no longer agree with the DMRG results because the umklapp scattering strength becomes very large. Due to the unconventional combination of the charge and spin degrees of freedom induced by the next-nearest-neighbor hopping, the system can accommodate a variety of physical phenomena unparalleled in the simple 1D Hubbard model. The region with two Fermi points is characterized by the $2k_F$ -SDW phase as in the case of $U = 2t_1$. However, the region with four Fermi points is drastically affected by the Coulomb interaction and the breakdown of the TLL state occurs near half filling. The strong-coupling phase diagram contains a large number of distinct metallic phases; namely, a paramagnetic metal, a spin-gapped liquid with incommensurate spiral correlations, a paramagnetic metal with strong ferromagnetic fluctuations, a fully-polarized ferromagnetic metal, a spin-singlet superconductivity, and a spin-triplet superconductivity.

In contrast to the weak-coupling phase diagram which predicts a spin-gapped liquid (or superconducting) phase when the system has four Fermi points, we have found that the spin gap vanishes in the substantial region in the strong-coupling phase diagram. The absence of the spin gap is derived by three types of ferromagnetic mechanisms. The first is the flat-band mechanism around the FP boundary and at low densities. A nearly flat band is realized since the two band minima are slightly occupied by electrons at low densities (or the band maximum at $k = 0$ is slightly occupied by holes near the FP boundary.) Thus, the ground state is stabilized as the fully polarized ferromagnetic state. The second is the three-site ring-exchange interaction for $t_2 \gtrsim t_1$ at intermediate filling, where all the triangles formed by the hopping integrals satisfy the ferromagnetic sign rule $t_1^2 t_2 > 0$.¹⁹ The ferromagnetic interaction is short ranged⁴³ and is not sufficient to make the system ferromagnetic. The third is the Nagaoka mechanism near half filling. Since the competing antiferromagnetic exchange interaction is large, the ground state is not fully polarized.

Concerning the superconductivity, we have found a

couple of new phases, which are absent in the weak-coupling limit. One is the spin-triplet superconducting phase for $t_2 \gtrsim t_1$, where the attractive interaction is caused by the gain in kinetic energy due to ring exchange of electrons. The other is the spin-singlet superconducting phase along the FP boundary near half filling, where the superconducting fluctuations are enhanced by large difference between two Fermi velocities. This state is also regarded as the doped zigzag-bond spin-gapped state.

Acknowledgments

This work was supported in part by Grants-in-Aid for Scientific Research (Nos. 18028008, 18043006, and 18540338) from the Ministry of Education, Science, Sports, and Culture of Japan. A part of computations was carried out at the Research Center for Computational Science, Okazaki Research Facilities, and the Institute for Solid State Physics, University of Tokyo.

-
- ¹ T. Ishiguro and T. Yamaji, *Organic superconductors* (Springer-Verlag, Berlin, 1990).
 - ² *Conjugated Conducting Polymers*, edited by H. Kiess (Springer-Verlag, Berlin, 1992).
 - ³ H. Kishida, H. Matsuzaki, H. Okamoto, T. Manabe, M. Yamashita, Y. Taguchi, and Y. Tokura, *Nature (London)* **405**, 929 (2000).
 - ⁴ M.C. Gutzwiller, *Phys. Rev. Lett.* **10**, 159 (1963).
 - ⁵ J. Hubbard, *Proc. R. Soc. London, Ser. A* **276**, 238 (1963).
 - ⁶ J. Kanamori, *Prog. Theor. Phys.* **30**, 275 (1963).
 - ⁷ E.H. Lieb and F.Y. Wu, *Phys. Rev. Lett.* **20**, 1445 (1968).
 - ⁸ F.D. Haldane, *Phys. Rev. Lett.* **45**, 1358 (1980); *J. Phys. C* **14**, 2585 (1981); *Phys. Lett. A* **81**, 153 (1981).
 - ⁹ K. Kuroki, R. Arita, and H. Aoki, *J. Phys. Soc. Jpn.* **66**, 3371 (1997).
 - ¹⁰ S. Daul and R.M. Noack, *Phys. Rev. B* **61**, 1646 (2000).
 - ¹¹ M.E. Torio, A.A. Aligia, and H.A. Ceccatto, *Phys. Rev. B* **67**, 165102 (2003).
 - ¹² G.I. Japaridze, R.M. Noack, and D. Baeriswyl, *cond-mat/0607054*.
 - ¹³ P. Pieri, S. Daul, D. Baeriswyl, M. Dzierzawa, and P. Fazekas, *Phys. Rev. B* **54**, 9250 (1996).
 - ¹⁴ S. Daul, P. Pieri, M. Dzierzawa, D. Baeriswyl, and P. Fazekas, *Physica B* **230-232**, 1021 (1997).
 - ¹⁵ S. Daul and R.M. Noack, *Z. Phys. B* **103**, 293 (1997).
 - ¹⁶ S. Daul and R.M. Noack, *Phys. Rev. B* **58**, 2635 (1998).
 - ¹⁷ M. Fabrizio, *Phys. Rev. B* **54**, 10054 (1996).
 - ¹⁸ R. Arita, K. Kuroki, H. Aoki, and M. Fabrizio, *Phys. Rev. B* **57**, 10324 (1998).
 - ¹⁹ Y. Ohta, S. Nishimoto, T. Shirakawa, and Y. Yamaguchi, *Phys. Rev. B* **72**, 012503 (2005).
 - ²⁰ W. Hofstetter, J.I. Cirac, P. Zoller, E. Demler, and M.D. Lukin, *Phys. Rev. Lett.* **89**, 220407 (2002).
 - ²¹ D. Jérôme, A. Mazaud, M. Ribault, and K. Bechgaard, *J. Phys.(France) Lett.* **41**, L95 (1980).
 - ²² K. Bechgaard, K. Carneiro, M. Olsen, F.B. Rasmussen, and C.S. Jacobsen, *Phys. Rev. Lett.* **46**, 852 (1981).
 - ²³ I.J. Lee, P.M. Chaikin, and M.J. Naughton, *Phys. Rev. B* **62**, R14669 (2000); *Phys. Rev. Lett.* **88**, 207002 (2002).
 - ²⁴ I.J. Lee, S.E. Brown, and M.J. Naughton, *J. Phys. Soc. Jpn.* **75**, 051011 (2006).
 - ²⁵ Y. Ohta, S. Nishimoto, T. Shirakawa, Y. Yamaguchi, *Physica B* **378**, 439 (2006).
 - ²⁶ M. Matsukawa, Y. Yamada, M. Chiba, H. Ogasawara, T. Shibata, A. Matsushita, and Y. Takano, *Physica C* **411**, 101 (2004).
 - ²⁷ S. Sasaki, S. Watanabe, Y. Yamada, F. Ishikawa, K. Fukuda, and S. Sekiya, *cond-mat/0603067*.
 - ²⁸ K. Sano, Y. Ôno, and Y. Yamada, *J. Phys. Soc. Jpn.* **74**, 2885 (2005).
 - ²⁹ K. Sano and Y. Ôno, *J. Phys. Soc. Jpn.* **76**, in press (2007).
 - ³⁰ T. Nakano, K. Kuroki, and S. Onari, *cond-mat/0701160*.
 - ³¹ R. Amasaki, Y. Shibata, and Y. Ohta, *Phys. Rev. B* **66**, 012502 (2002).
 - ³² S. Nishimoto and Y. Ohta, *Phys. Rev. B* **68**, 235114 (2003).
 - ³³ Y. Nagaoka, *Phys. Rev.* **147**, 392 (1966).
 - ³⁴ D.C. Mattis and R.E. Peña, *Phys. Rev. B* **10**, 1006 (1974).
 - ³⁵ M. Sigrist, H. Tsunetsugu, K. Ueda, and T.M. Rice, *Phys. Rev. B* **46**, 13838 (1992).
 - ³⁶ E. Müller-Hartmann, T. Hanisch, and R. Hirsch, *Physica B* **186-188**, 834 (1993).
 - ³⁷ H.J. Schulz, *Phys. Rev. Lett.* **64**, 2831 (1990).
 - ³⁸ K. Sano, *J. Phys. Soc. Jpn.* **69**, 1000 (2000).
 - ³⁹ J. Voit, *Rep. Prog. Phys.* **58**, 977 (1995).
 - ⁴⁰ S. Ejima, F. Gebhard, and S. Nishimoto, *Europhys. Lett.* **70**, 492 (2005).
 - ⁴¹ H. Frahm and V.E. Korepin, *Phys. Rev. B* **42**, 10553 (1990).
 - ⁴² H.J. Schulz, *Phys. Rev. B* **53**, R2959 (1996).
 - ⁴³ S. Nishimoto, T. Shirakawa, and Y. Ohta,

- cond-mat/0701579.
- ⁴⁴ S.R. White, Phys. Rev. Lett. **69**, 2863 (1992); Phys. Rev. B **48**, 10345 (1993).
 - ⁴⁵ L. Balents and M.P.A. Fisher, Phys. Rev. B **53** 12133 (1996).
 - ⁴⁶ R. Eder and Y. Ohta, Phys. Rev. B **56**, R14247 (1997).
 - ⁴⁷ C. Gros, K. Hamacher, and W. Wenzel, Europhys. Lett. **69**, 616 (2005).
 - ⁴⁸ P. Sengupta, A.W. Sandvik, and D.K. Campbell, Phys. Rev. B **65**, 155113 (2002).
 - ⁴⁹ F.D.M. Haldane, Phys. Rev. B **25**, 4925 (1982).
 - ⁵⁰ K. Okamoto and K. Nomura, Phys. Lett. A **169**, 433 (1996).
 - ⁵¹ S. Eggert, Phys. Rev. B **54**, R9612 (1996).
 - ⁵² S. White and I. Affleck, Phys. Rev. B **54**, 9862 (1996).
 - ⁵³ J. Voit, Phys. Rev. B **45**, 4027 (1992).
 - ⁵⁴ K. Okunishi, Phys. Rev. B **75**, 174514 (2007).
 - ⁵⁵ F. Gebhard and X. Zotos, Phys. Rev. B **43**, 1176 (1991).